JOURNAL OF GEOPHYSICAL RESEARCH, VOL. 106, NO. A6, PAGES 10,519–10,535, JUNE 1, 2001

Quasi-linear Zakharov simulations of Langmuir turbulence at rocket altitudes in the auroral ionosphere

K. Y. Sanbonmatsu

Los Alamos National Laboratory, Los Alamos, New Mexico

D. L. Newman and M. V. Goldman

Center for Integrated Plasma Studies, University of Colorado at Boulder, Boulder, Colorado

Abstract. A quasi-linear Zakharov simulation model has been constructed to study intense Langmuir waves and precipitating field-aligned electrons observed in the auroral ionosphere at altitudes below 1000 km. This self-consistent model couples the magnetized Zakharov equations to a modified quasi-linear diffusion equation, which includes an advective term describing electrons streaming into the simulation region. Two-dimensional beam-driven simulations demonstrate that for the parameters of the auroral ionosphere below altitudes of 1000 km, Langmuir wave-wave and wave-particle interactions occur on similar timescales. The resulting reduced electron distribution has multiple shoulders and is a result of a balance between quasi-linear beam-flattening, wave-wave instabilities and beam replenishment due to streaming electrons.

1. Introduction

Electron streams are unstable to the excitation of Langmuir waves in many space plasma environments, such as the auroral ionosphere [*McFadden et al*., 1986], the solar wind [*Lin et al*., 1986], and the Earth's electron foreshock [*Kellogg and Monsoon*, 1978]. In the auroral ionosphere at rocket altitudes, intense bursts of Langmuir waves are detected in conjunction with transient, field-aligned electron fluxes, with shoulder-like features in the reduced parallel electron velocity distribution (i.e., the electron velocity distribution integrated over velocities perpendicular to the background **B** field). The sounding rockets of the University of California, Berkeley, have observed both large-amplitude Langmuir waves ($E \approx 50$–500 mV m^{-1}) and energetic, field-aligned electrons (100 eV to 3 keV) at altitudes near 700 km [*McFadden et al*., 1986; *Boehm*, 1987; *Ergun et al*., 1991]. These bursts of Langmuir waves typically have been in the range of 20–100 ms in duration and have amplitudes large enough to suggest that wave-wave effects may be important. The reduced electron distributions associated with these bursts sometimes have multiple shoulder features [*Ergun et al*., 1993]. The Freja satellite has made similar Langmuir wave measurements at higher altitudes (1700 km), reporting Langmuir wave amplitudes of several hundred mV m^{-1} [*Kintner et al*., 1995] and even as high as 1 V m^{-1} in some cases [*Stasiewicz et al*., 1996].

The Langmuir wave emissions are thought to arise from modulations in the electron flux which produce a transient positive slope in the reduced electron velocity distribution via velocity dispersion [*Ergun et al*., 1993]. Sounding rockets typically have insufficient time resolution to detect this transient positive slope in the reduced electron distribution and instead measure time-averaged reduced electron distributions with shoulders which are rarely if ever observed to have positive slopes. They do, however, detect positive slopes in parallel (to the geomagnetic field) cuts of the electron distribution as well as evidence for velocity dispersion [*Ergun et al*., 1993]. This is not surprising since the time it takes to measure a distribution cut is much shorter than the time to measure a reduced distribution. A positive slope in a parallel cut of the distribution, however, does not imply instability. Hence the process of Langmuir wave excitation and the subsequent saturation of this instability cannot be observed directly and remain poorly understood.

The rarity of observations with a well-defined positive slope in the reduced electron distribution suggests that waves driven by such an unstable distribution will remove the positive slope through wave-particle interactions (i.e., quasi-linear beam flattening). However, the advection of "fresh" electrons into the region can act to restore this positive slope (beam replenishment). Furthermore, the excited Langmuir waves can be unstable to wave-wave interactions, in which they may backscatter. In this case, they will no longer be in resonance with electrons near the beam velocity $v \approx v_b$ (i.e., the region of the electron distribution with positive slope). The backscattered waves act to flatten the distribution near $v \approx -v_b$ instead of flattening regions near $v \approx v_b$. Because beam-resonant Langmuir energy is transferred to Langmuir waves that are not beam resonant, backscatter has the net effect of reducing the rate at which the beam's slope in velocity space is decreased (quasi-linear beam flattening).

In effect, this backscatter weakens quasi-linear flattening of the beam. If the wave-wave interaction timescale were much faster than that of wave-particle interactions, excited Langmuir waves would be removed from resonance with the beam so quickly that the beam would never flatten. In the opposite timescale ordering, the beam would flatten before any backscatter could occur. Our model shows that for the parameters of the auroral ionosphere near 700 km altitude, a balance occurs between quasi-linear beam flattening, Langmuir wave-wave interactions, and beam replenishment, resulting from the fact that the wave-particle and wave-wave effects occur on similar timescales. While the excited Langmuir waves cause

Paper number 2000JA000270.
0148-0227/01/2000JA000270$09.00

significant velocity diffusion of the beam, replenishment maintains a weakly unstable feature in the reduced distribution, sustaining Langmuir waves (via growth due to the bump-on-tail instability) for many milliseconds.

Particle-in-cell (PIC) simulations are capable of simulating both wave-particle and wave-wave effects simultaneously, although these simulations (which must be two-dimensional in order to include magnetized Langmuir waves relevant to the auroral ionosphere) are typically too noisy to study the extremely weak (i.e., beam growth rate $\gamma \ll \omega_{pe}$ and beam density $n_b \ll n_0$, where n_0 is the background density) electron beams in the auroral ionosphere (for example, our quasi-linear Zakharov simulations show a near–steady state growth rate of $\gamma/\omega_{pe} \approx 2 \times 10^{-4}$ at late times). Furthermore, PIC simulations are usually too computationally demanding to use realistic electron-ion mass ratios for realistic simulation times (10–100 ms or 6×10^4–$6 \times 10^5 \omega_{pe}^{-1}$). Limited work has been done concerning weak beam instabilities in a two-dimensional (2-D) magnetized plasma using PIC simulations [*Dum and Nishikawa*, 1994]. However, these have been limited by their noise level and relied on initializing the system with a cold beam.

Vlasov simulations also include wave-particle and wave-wave effects, but are too demanding to run in 2-D, required by the magnetized environment of the auroral ionosphere for the necessary long timescales. Previous studies of quasi-linear diffusion in the auroral ionosphere [*Muschietti et al*., 1997] have neglected wave-wave interactions, which we demonstrate in this work to be important in modeling the observed large-amplitude Langmuir waves. Zakharov (partial differential equation) simulations have been performed to model auroral Langmuir wave-wave effects; however, these assume a fixed electron distribution and neglect the back reaction of excited waves on the electron distribution [*Newman et al*., 1994b].

Studies performed by *Muschietti and Dum* [1991] have compared wave-wave and wave-particle effects. However, these studies have been one dimensional and have neglected the magnetic effects which can be important in describing the evolution of the Langmuir wave spectrum [*Newman et al*., 1994b]. Other simulations have compared wave-wave and wave-particle effects for inertial confinement fusion applications [*Thomson et al*., 1973, 1974]; however, these were 1 D and not self-consistent. Furthermore, these simulations modeled the evolution of a Maxwellian particle distribution driven by a laser, rather than the bump-on-tail instability.

To study the interaction between observed Langmuir wave bursts and precipitating field-aligned electrons, we present a simulation model which includes both wave-wave and wave-particle effects. This self-consistent model couples a magnetized generalization of the Zakharov equations [*Zakharov and Shabat*, 1972; *Newman et al*., 1994b] with a modified quasi-linear equation for the electron distribution, which allows us to study extremely weak precipitating electron beams. The quasi-linear equation is modified to include a term representing the advection of electrons into the simulation region. A similar model has been applied to inertial confinement fusion for the case of unmagnetized one-dimensional Langmuir waves and has been validated against particle-in-cell simulations [*Sanbonmatsu et al*., 1999, 2000a, 2000b].

In this work, we demonstrate that both wave-wave and wave-particle effects can interact to produce shoulders both parallel and antiparallel to the beam direction, resulting from a combination of nonlinear wave-wave scattering and quasi-linear diffusion of the electron distribution. The balance of this work is organized as follows: First, we describe the quasi-linear Zakharov model in detail. Next, we present the parameters and initial conditions for our simulations. We then present the simulation results obtained from the quasi-linear Zakharov model, as applied to the auroral ionosphere for altitudes near 700 km, compare with observations, and discuss the implications of our results.

2. Quasi-linear Zakharov Model

2.1. Modified Quasi-linear Diffusion

The quasi-linear diffusion equation evolves the spatial average of the particle velocity distribution function and is obtained by taking the spatial average of the Vlasov equation. Below we justify neglecting the off-diagonal components of the quasi-linear diffusion tensor for the special case of magnetized Langmuir waves in the auroral ionosphere and subsequently motivate the advective beam replenishment term in the case of parallel diffusion.

In a uniform background magnetic field $\mathbf{B}_0$ the standard quasi-linear diffusion equation is

$$\partial_t F_e(\mathbf{v}, t) = \partial_{\mathbf{v}} \cdot \mathbf{D}(\mathbf{v}, t) \cdot \partial_{\mathbf{v}} F_e(\mathbf{v}, t), \tag{1}$$

where $F_e(\mathbf{v}, t)$ is the spatially averaged (over volume V) particle distribution function and the quasi-linear diffusion tensor $\mathbf{D}(\mathbf{v}, t)$ is

$$\mathbf{D}(\mathbf{v}, t) = \lim_{V \to \infty} \frac{4\pi^2 e^2}{v_z V m_e^2} \sum_{n=-1}^{1} \int_0^\infty k_\perp \, dk_\perp \, |\mathbf{E}_k(t)|^2 J_n^2(b) \, \frac{\mathbf{a}_n \mathbf{a}_n}{k^2}, \tag{2}$$

where the J_n are the Bessel functions with arguments $b = k_\perp v_\perp / \omega_{ce}$ [*Shapiro and Shevchenko*, 1962; *Kennel and Engelmann*, 1966]. While this standard form takes the limit of an infinite spatial domain, we treat the case of a finite spatial domain with dimension parallel to the magnetic field of length L and perpendicular to the magnetic field of length $L_\perp$. The factor $\mathbf{a}_n$ is defined by $\mathbf{a}_n = (n\omega_{ce}/v_\perp)\hat{\mathbf{e}}_\perp + k_z \hat{\mathbf{e}}_z$, where $\hat{\mathbf{e}}_\perp$ and $\hat{\mathbf{e}}_z$ are unit vectors in the directions perpendicular and parallel to the magnetic field, respectively. The factors $\mathbf{a}_n$ and k_z are evaluated at resonance, $k_z v_z = \omega_r - n\omega_{ce}$. In the auroral ionosphere the electrons are strongly magnetized, in the sense that $k_\perp^2 \rho_e^2 \ll 1$, where $\rho_e \equiv v_e/\omega_{ce}$ is the electron Larmor radius of a thermal electron and v_e is the electron thermal velocity. This allows us to keep only the Čerenkov (i.e., Landau), Doppler (i.e., Doppler-shifted cyclotron resonance), and anomalous Doppler resonances in (2) (i.e., $n = 0, \pm 1$). Although the electrons are strongly magnetized, the Langmuir waves are only moderately magnetized in the sense that $\omega_{ce} \approx \omega_{pe}$ ($\omega_{ce} = 1.2\omega_{pe}$ for the case considered in this work). As is usual in the quasi-linear approximation, terms corresponding to additional nonlinear effects such as trapping are neglected since they are higher order in $E(z, t)$.

When we calculate the diffusion tensor components, we find the perpendicular components to be exponentially small compared with the parallel components for parameters of the auroral ionosphere near 700 km. This has been previously verified using test particle simulations [*Sanbonmatsu et al*., 1997]. Since perpendicular diffusion is much slower than diffusion along the magnetic field lines, we can reduce the diffusion equation to 1 D, along magnetic field lines:

$$\partial_t F_e(v_z, t) = \partial_{v_z} D_{zz}(v_z, t) \partial_{v_z} F_e(v_z, t), \quad (3)$$

where the diffusion coefficient is now the parallel-parallel component of the diffusion tensor and is proportional to the integrated 2-D wave spectrum

$$D_{zz}(v_z, t) = \frac{4\pi^2 e^2}{v_z L L_\perp m_e^2} \int_0^\infty k_\perp \, dk_\perp \, |k\psi(k_\perp, k_z = \omega/v_z, t)|^2 \quad (4)$$

and we consider the finite spatial domain with parallel extent L and perpendicular extent $L_\perp$. The nonresonant contribution is negligible for the parameters used in this work. The slowly varying envelope potential ψ (used in the Zakharov part of the model) is defined by $\mathbf{E} = -\nabla\psi$, where $\mathbf{E}$ is the slowly varying envelope of the electric field $\tilde{\mathbf{E}}$ defined by $\tilde{\mathbf{E}} = (\mathbf{E}e^{-i\omega_{pe}t} + \text{c.c.})/2$. Beam replenishment is modeled by source and sink terms in the quasi-linear diffusion equation, which come from the spatial average over a finite spatial domain (length L) of the advective term in the Vlasov equation (this term goes to zero in the standard quasi-linear derivation where an infinite spatial domain is considered).

The complete derivation of the quasi-linear Zakharov model is presented in the appendix of *Sanbonmatsu et al*. [2000b] with explicit treatment of the two-timescale approximation in the quasi-linear diffusion equation. Here we present a brief motivation of the replenishment term used in our modified quasi-linear diffusion equation. The 1-D Vlasov equation is

$$\partial_t f_e(z, v_z, t) + v_z \partial_z f_e(z, v_z, t) - \frac{e}{m_e} E_z \partial_{v_z} f_e(z, v_z, t) = 0. \quad (5)$$

Taking the spatial average over length L gives

$$\partial_t F_e(v_z, t) + \frac{v_z}{L}[f_e^+(v_z, t) - f_e^-(v_z, t)] = \frac{e}{m_e}\frac{1}{L}\int_{-L/2}^{L/2} dz \, E(z, t) \partial_{v_z} \delta f_e(z, v_z, t), \quad (6)$$

where $F_e(v_z, t)$ is the spatial average, $\delta f_e(z, v_z, t) = f_e(z, v_z, t) - F_e(v_z, t)$ represents spatial deviations from the average, $f_e^+(v_z, t) = f_e(z = L/2, v_z, t)$, and $f_e^-(v_z, t) = f_e(z = -L/2, v_z, t)$. Next, we substitute the k-space Fourier representations of $E(z, t)$ and $\delta f_e(z, v_z, t)$, solve for $\delta f_e(z, v_z, t)$ in terms of $F_e(v_z, t)$, and subtract (6) from (5) (this is the standard method used to derive the quasi-linear diffusion equation). We obtain a modified version of the quasi-linear diffusion equation:

$$\partial_t F_e(v_z, t) = \partial_{v_z} D_{zz}(v, t) \partial_{v_z} F_e(v_z, t) - \frac{v_z}{L}[f_e^+(v_z, t) - f_e^-(v_z, t)], \quad (7)$$

where the second and third terms on the right-hand side come from the advective term in the Vlasov equation and represent electrons entering and exiting the region over which the spatial average is taken.

We assume a bump-on-tail distribution for the electrons entering region L at the left. This models the precipitating electrons in the auroral zone entering a spatial region from above. We assume the same bump-on-tail distribution for the initial condition of the spatial average $F_e(v_z, t = 0)$. Thus, initially, a pristine warm beam exists throughout region L. These assumptions give $f_e^-(v_z, t) = F_e(v_z, t = 0)$ for $v_z > 0$ and $f_e^+(v_z, t) = F_e(v_z, t = 0)$ for $v_z < 0$. We also assume that the distribution of electrons leaving region L is approximately equal to the average over L. That is, $f_e^+(v_z, t) = F_e(v_z, t)$ for $v_z > 0$ and $f_e^-(v_z, t) = F_e(v_z, t)$ for $v_z < 0$. This assumption has been verified by fully kinetic particle-in-cell simulations applied to laser-plasma interactions in inertial confinement fusion [*Sanbonmatsu et al*., 1999, 2000a, 2000b].

The modified quasi-linear diffusion equation now becomes

$$\partial_t F_e(v_z, t) = \partial_{v_z} D_{zz}(v, t) \partial_{v_z} F_e(v_z, t) - \frac{|v_z|}{L}[F_e(v_z, t) - F_e(v_z, t = 0)]. \quad (8)$$

Physically, the advective terms on the right-hand side have the effect of restoring the distribution to its original state, i.e., a warm beam. It is in this sense that the beam is replenished. The length L controls the strength of the replenishment. We refer to L as the replenishment length, which is bounded above by the length scales L_{grad} for the gradients of the background plasma parameters (n_0, λ_e, ω_{ce}, and ω_{pe}) in the auroral ionosphere and bounded below by the length L_{waves} corresponding to the maximum resolution in k space ($L_{\text{waves}} = 2\pi/\Delta k_z$) used in the Zakharov part of our simulations. That is, we require $L_{\text{waves}} \ll L \ll L_{\text{grad}}$. Approximating the exiting electron distribution by the spatial average will have the effect of underestimating the strength of the replenishment terms. We also note that the replenishment rate is proportional to $|v_z|$. Physically, the rate at which the beam is restored is proportional to the flux of entering particles, causing replenishment at higher velocities to occur more quickly.

2.2. Magnetized Zakharov Equations

The 2-D magnetized Zakharov equations, which describe the mutual nonlinear interaction of high-frequency magnetized Langmuir waves with low-frequency density perturbations, are [*Krasnoselskikh and Sotnikov*, 1977; *Newman et al*., 1994b]

$$\nabla^2\left(i\partial_t + \frac{3}{2}\omega_{pe}\lambda_e^2\partial_z^2 + i\hat{\gamma}_L\right)\psi - \frac{1}{2}\frac{\omega_{ce}^2\omega_{pe}}{\omega_{ce}^2 - \omega_{pe}^2}\partial_\perp^2\psi = \frac{\omega_{pe}}{2n_o}\nabla(\delta n \nabla\psi), \quad (9)$$

$$(\partial_t^2 - c_s^2\nabla^2 + 2i\hat{\gamma}_{ia}\partial_t)\delta n = \frac{1}{16\pi m_i}\nabla^2|\nabla\psi|^2. \quad (10)$$

We assume the low-frequency density response δn to be ion acoustic waves or ion acoustic quasi-modes with damping rate $\hat{\gamma}_{ia}$, which is assumed to be linear in the ion acoustic frequency kc_s with the constant of proportionality determined by the electron to ion temperature ratio T_e/T_i, where c_s is the ion sound speed similar to *Newman et al*. [1994b]. The magnetized Zakharov equations were discussed in detail by *Newman et al*. [1994b].

The operator $\hat{\gamma}_L$ corresponds to growth (damping for $\hat{\gamma}_L < 0$) of Langmuir waves in a magnetized plasma due to the reduced electron distribution $F_e(v_z, t)$ and has the k-space representation [*Clemmow and Dougherty*, 1969]

Table 1. Auroral Ionosphere Simulation Parameters

Parameter	Symbol	Value	Units
Altitude		700	km
Gyroradius	ρ_e	2.75	cm
Plasma frequency	f_{pe}	0.95	MHz
Cyclotron frequency	f_{ce}	1.15	MHz
Frequency ratio	ω_{ce}/ω_{pe}	1.2	
Electron bulk density	n_e	10^4	cm^{-3}
Electron temperature	T_e	0.2 ± 0.05	eV
Ion temperature	T_i	0.05	eV
Electron thermal speed	v_e	1.79×10^7	cm s^{-1}
Electron Debye length	λ_e	3.3	cm
Beam density	n_b/n_e	0.0005	
Beam velocity	v_b/v_e	40	
Beam thermal velocity	$\Delta v_b/v_e$	6	
Halo density	n_h/n_e	0.035	
Halo thermal velocity	θ/v_e	6	
Replenishment length	L	24	km
Wave simulation length	L_{waves}	0.14	km
Halo exponent	β	5	

$$\gamma_L(k_\perp, k_z, t) = \frac{1}{\partial_\omega \varepsilon_r} \operatorname{Im}\left(\frac{\omega_{pe}^2}{k^2} \int d^3\mathbf{v} \sum_{n=\infty}^{\infty} J_n^2(b) \frac{k_z \partial_{v_z} f_e + \frac{n}{b} k_\perp \partial_{v_\perp} f_e}{\omega - n\omega_{ce} - k_z v_z} \right). \quad (11)$$

The specific form of (11) used in our simulations is dependent on the electron distribution and is discussed in section 3.1 in detail in the context of the electron distribution used in our simulations. Equation (11) requires $\gamma_L \ll \omega_{pe}$, which is well satisfied for our simulations. The real part of the dielectric function $\varepsilon_r = \text{Re}\,[\varepsilon(\omega_r, \mathbf{k})]$ is evaluated at the real frequency $\omega = \omega_r$ [*Newman et al*., 1994a]. A cold fluid approximation is used for this factor since the kinetic contribution to ε_r is negligible for ionospheric electron velocity distributions and since the Langmuir wave spectra considered in this work have $k^2\lambda_e^2 \ll 1$.

The Zakharov portion of the quasi-linear Zakharov simulation is the same as that used in the wave-wave studies by *Newman et al*. [1994b, 1990] and *Robinson and Newman* [1990, 1988]. This method uses the pseudospectral technique to evolve the Cartesian finite difference version of (9)–(10) in 2-D k space.

2.3. Coupled Wave and Particle Evolution

Equations (8)–(11) comprise the quasi-linear-Zakharov model. Equation (8) describes the evolution of the spatially averaged reduced electron velocity distribution due to the wave spectrum, which enters into the diffusion coefficient $D_{zz}(v_z, t)$. The magnetized Zakharov equations (9)–(10) evolve the wave spectrum according to the time-evolving growth rate $\gamma_L(k_\perp, k_z, t)$, determined from the electron distribution.

The quasi-linear Zakharov model has the following requirements for validity: The quasi-linear equation (8) requires the autocorrelation time of the wave spectrum to be much smaller than the diffusion time of the electron distribution ($t_{ac} \ll t_D$). To justify use of the 1-D quasi-linear equation (8), perpendicular diffusion must be negligible (i.e., $D_{\perp\perp}, D_{\perp z}, D_{z\perp} \ll D_{zz}$). The validity of these assumptions for quasi-linear diffusion near 700 km in the auroral ionosphere was verified and discussed at length by *Sanbonmatsu et al*. [1997] for wave spectra similar to those produced in the simulations described here. The Zakharov equations (9)–(10) require the ratio of wave energy to thermal energy to be small ($|E|^2/8\pi n_0 T_e \ll 1$) in order to neglect higher-order nonlinearities. Furthermore, the two-timescale approximation requires the dispersive terms in (9) to be small. That is, $k^2\lambda_e^2 \ll 1$ and $k_\perp \ll k_z$ for $\omega_{ce} = 1.2\omega_{pe}$. All of the above approximations are well satisfied in our simulations.

3. Simulations

3.1. Boundary and Initial Conditions

The parameters used in our simulations are determined from measurements made by the Bidarca Berkeley sounding rocket [*Ergun et al*., 1991]. Table 1 lists the values of the parameters used in our simulations. The electron plasma and cyclotron frequencies are calculated from the observed electron density and magnetic field, respectively. The electron and ion temperatures are estimated from observed velocity distributions, as are the electron Debye length and thermal velocity.

The model electron velocity distribution used as an initial condition in our simulations is based on the electron distributions observed by the Bidarca spacecraft at altitudes near 700 km and is similar in form to that used by *Muschietti et al*. [1997]. The 2-D distribution (Figure 1) takes the form:

$$f_e(v_\perp, v_z, t=0) = f_0(v_\perp, v_z) + f_h(v_\perp, v_z) + f_b(v_\perp, v_z), \quad (12)$$

$$f_0(v_\perp, v_z) = \frac{n_0}{(2\pi v_e^2)^{3/2}} \exp\left[-(v_\perp^2 + v_z^2)/2v_e^2\right],$$

$$f_h(v_\perp, v_z) = \frac{3n_h}{2\pi^2\theta^3} \frac{1}{\left[1 + (v_\perp^2 + v_z^2)/\theta^2\right]^{\beta/2}},$$

$$f_b(v_\perp, v_z) = \frac{n_b}{(2\pi)^{3/2}\Delta v_{b_z}\Delta v_{b_\perp}^2} \exp\left[-(v_z - v_b)^2/2\Delta v_{b_z}^2\right] \exp\left[-v_\perp^2/2\Delta v_{b_\perp}^2\right],$$

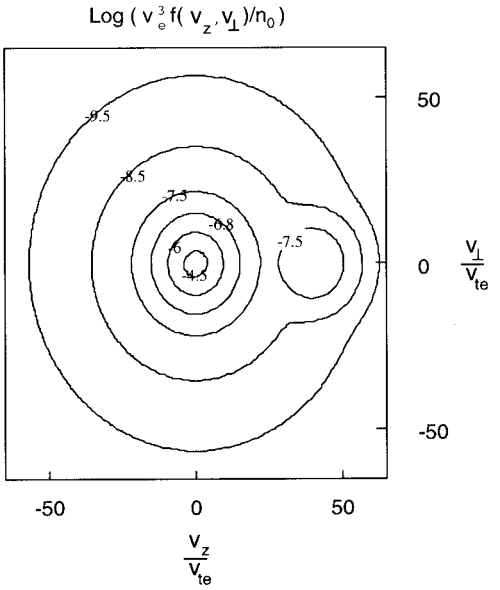

Figure 1. Initial 2-D electron velocity distribution used in simulations.

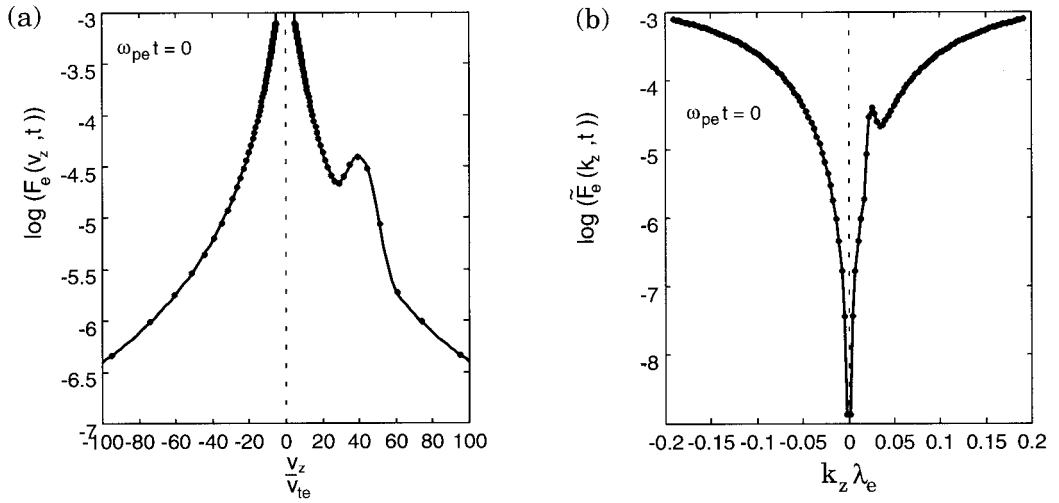

Figure 2. Initial condition for simulation: (a) Reduced 1-D electron velocity distribution for parameters in Table 1. (b) Reduced distribution in k space, assuming resonance $\omega = k_z v_z$, where $k_z\lambda_e \ll 1$ and $k_\perp \ll k_z$. The solid circles on the curves represent the simulation grid.

where $f_0(v_\perp, v_z)$ is the bulk of the distribution ($n_0 \gg n_h, n_b$), $f_h(v_\perp, v_z)$ is the background isotropic halo component (due to scattered electrons), and $f_b(v_\perp, v_z)$ is the beam component. The isotropic halo f_h (due to scattered electrons [see *Newman et al*. [1994a]) is modeled by a generalized Lorentzian function which falls off as $v^{-\beta}$ and has width θ. The generalized Lorentzian is also known as a κ function, where $\kappa \equiv \beta/2 - 1$ [*Mace and Hellberg*, 1995]. Previous treatments have employed a simple power law (i.e., $f_h \propto v^{-\beta}$); however, power law distributions are not normalizable and thus require an artificial cutoff velocity at some $v_{\min}$ [*Newman et al*., 1994b; *Muschietti et al*., 1997]. The parameters v_b, Δv_b, and n_b of the Maxwellian beam distribution f_b are chosen so that after flattening via quasi-linear diffusion the evolved distribution resembles the primary shoulder in observed electron distributions. We note that the other secondary shoulders observed in our simulation results (discussed in detail in section 3.2) and in spacecraft data are not present in our initial model electron distribution. These secondary shoulders are produced self-consistently by a combination of wave-wave and wave-particle processes and emerge at late times in our simulations.

Since the quasi-linear Zakharov model evolves the reduced 1-D electron velocity distribution, (12) must be integrated over perpendicular velocity $v_\perp$ (recall that it is positive slope in the reduced 1-D electron distribution rather than the distribution itself that produces Langmuir wave growth). This gives

$$F_e(v_z, t = 0) = F_0(v_z) + F_h(v_z) + F_b(v_z), \tag{13}$$

$$F_0(v_z) = \frac{n_0}{\sqrt{2\pi}v_e} \exp(-v_z^2/2v_e^2),$$

$$F_h(v_z) = \frac{n_h}{\pi\theta} \frac{1}{(1 + v_z^2/\theta^2)^{\beta/2-1}},$$

$$F_b(v_z) = \frac{n_b}{\sqrt{2\pi}\Delta v_{b_z}} \exp[-(v_z - v_b)^2/2\Delta v_{b_z}^2].$$

We note that the integrand in the integration over $v_\perp$ must have a $J_0(k_\perp v_\perp/\omega_{ce})^2$ weighting factor to obtain the proper form of the Langmuir wave growth rate to be used in the magnetized Zakharov equations. However, our Langmuir spectra have $k_z\lambda_e \ll 1$ and $k_\perp \gg k_z$. Since $\omega_{pe} \approx \omega_{ce}$ at 700 km, $k_\perp v_\perp \approx k_\perp v_e \ll \omega_{ce}$, making $k_\perp v_\perp \ll \omega_{ce}$ and the weighting factor $J_0 \approx 1$.

The model reduced 1-D electron distribution is shown in Figure 2 as a function of velocity (Figure 2a) and of wave number (Figure 2b) assuming resonance $\omega \approx \omega_{pe} = k_z v_z$. This approximation is valid for the Langmuir spectra in our simulations which have $k^2\lambda_e^2 \ll 1$ and $k_\perp \ll k_z$. Since the nonresonant contributions are always negligible, the quasi-linear and Zakharov equations are solved in k space using $\omega \approx k_z v_z$. The solid circles correspond to the simulation grid which is uniform in k_z but becomes nonuniform when mapped to velocity space.

Using (13) as the form for the electron distribution reduces the Langmuir wave growth rate to [*Shapiro and Shevchenko*, 1988]

$$\gamma_L(k_\perp, k_z, t) = \frac{\pi}{\partial_\omega \varepsilon_r} \frac{\omega_{pe}^2}{k_z^2} \left[\cos^2\tilde{\theta}\, \partial_{v_z} F_e\left(v_z = \frac{\omega_{pe}}{k_z}\right) - \frac{k_z}{2\omega_{ce}} \sin^2\tilde{\theta} F_e\left(v_z = \frac{\omega - \omega_{ce}}{k_z}\right) \right], \tag{14}$$

where $\tilde{\theta} = \tan^{-1}(k_\perp/k_z)$. The first term represents the Čerenkov resonance ($n = 0$), and the second term represents the first Doppler resonance ($n = 1$). Since there is a negligible number of particles near the anomalous Doppler resonance ($v_z \approx 88 v_e$ for $k_z \approx k_b \equiv \omega_{pe}/v_b$ and $n = -1$), the $n = -1$ term is neglected. Terms with $|n| \geq 2$ are neglected since they are higher than second order in $k_\perp v_\perp/\omega_{ce}$ and $k_\perp^2 v_\perp^2/\omega_{ce}^2 \ll 1$.

The initial Langmuir wave growth rate $\gamma_L(k_z, k_\perp, t = 0)$ is shown in 1-D slices in Figures 3a and 3b. In Figure 3a we see the growth rate as a function of k_z evaluated at $k_\perp = 0$. The maximum growth rate ($\gamma_L \approx 4.5 \times 10^{-3}$) lies near $k_z\lambda_e = 0.0285$, which corresponds to $v_z/v_e = 35.1$, i.e., the velocity at which the slope of the reduced electron distribution is maximum (see Figure 2). After examining only those k_z for which γ_L is positive (i.e., growth as opposed to damping), we see that there is a finite width to the growth. This is due to the finite

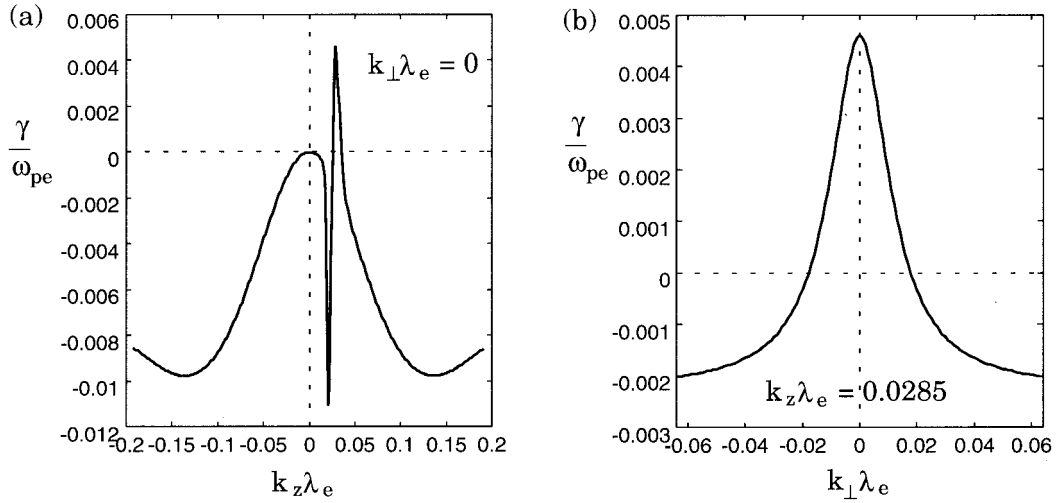

Figure 3. (a) One-dimensional slice of initial growth rate $\gamma_L(k_z, k_\perp = 0, t = 0)$ plotted as a function of k_z. (b) One-dimensional slice of initial growth rate $\gamma_L(k_z = k_{z,\max}, k_\perp, t = 0)$ plotted as a function of $k_\perp$, evaluated at the k_z which maximizes the growth rate ($k_z\lambda_e \approx 0.0285$).

region of positive slope in the reduced electron distribution $25 < v_z/v_e < 40$. The large dip to the left of the growth region corresponds to the large damping for $v_z > v_b$. The near-zero γ_L at $k_z = 0$ is due to the falloff of the damping rate as $v_z \to \infty$. Finally, the large damping at high $|k_z\lambda_e|$ is due to low velocities in the bulk of the reduced electron distribution.

Figure 3b shows the growth rate as a function of $k_\perp$ for the $k_z = k_{z,\max}$ at which the growth is maximum ($k_z\lambda_e = 0.0285$). The positive growth ($\gamma_L > 0$) region is due to the positive slope of the beam in the reduced electron distribution. The damped regions ($\gamma_L < 0$), however, are mainly due to the halo component of the reduced electron distribution interacting through the Doppler resonance.

The initial wave spectrum consists of white noise electric field fluctuations and allows fluctuations in δn to develop self-consistently. The boundary conditions for the Zakharov part of the simulation are periodic. In order to approximate the wave turbulence as statistically homogeneous the wave simulation box must be small compared with the replenishment length so that the wave simulation box represents a typical small subregion L_{waves} of the larger region L. The simulation has k-space resolution $\Delta k_z\lambda_e = 0.0015$, giving $L_{\text{waves}} = 4200\lambda_e \approx 0.14$ km. The replenishment length is chosen to be $L = 24$ km, consistent with the requirement that $L_{\text{waves}} \ll L \ll L_{\text{grad}}$. While this value of L is within the constraints, the choice of L is somewhat arbitrary. The effect of varying L on the simulation results is discussed in section 4.

3.2. Evolution of Wave Spectrum and Electron Distribution

Our simulation runs have two stages, which are described in detail in sections 3.3 and 3.4. Initially, the bump-on-tail instability produces a burst of intense Langmuir waves, which diffuse the beam in velocity space (via quasi-linear diffusion) and also scatter to modes that are not beam resonant, where they undergo Landau damping and distort the electron distribution through quasi-linear diffusion. As seen in Figure 4, the initial stage lasts approximately 3.4 ms, or $20{,}000\omega_{pe}^{-1}$. Subsequently, at late times in the simulations a balance between beam replenishment, beam flattening, and wave-wave backscatter is achieved. The beam replenishment maintains a small but finite positive slope in the reduced electron distribution, which, in turn, sustains a near–steady state Langmuir wave level. We have run our simulations out to 47 ms or $285{,}000\omega_{pe}^{-1}$, where we still observe a near-steady state in the average electrostatic energy.

Figure 5 displays the time evolution of the reduced electron velocity distribution. At early times the initial beam flattens. Two secondary shoulders emerge in the antiparallel direction between $t = 13{,}200\omega_{pe}^{-1}$ and $t = 26{,}000\omega_{pe}^{-1}$ and subsequently relax. At late times the distribution consists of the flattened beam, a secondary parallel shoulder, and a secondary antiparallel shoulder. These features are explained in detail in terms of the wave spectra below.

The distortion of the electron distribution is seen more clearly in k space. Plate 1 displays the time history of both the wave energy and the reduced electron distribution, allowing us to see clearly that wave-particle and wave-wave effects act on similar timescales. In Plate 1 the horizontal axis is parallel wave number k_z. The depth axis is time. In this case we display times $1 < \omega_{pe}t < 45{,}000$. The vertical axis is the natural log of the reduced k-space electron distribution (mapped from velocity

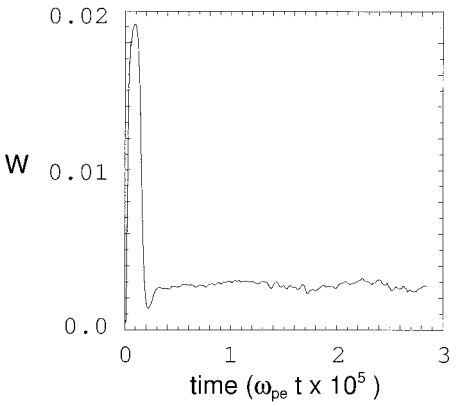

Figure 4. Time history of the average electric field strength in dimensionless units ($W = |E|^2/8\pi n_0 T_e$).

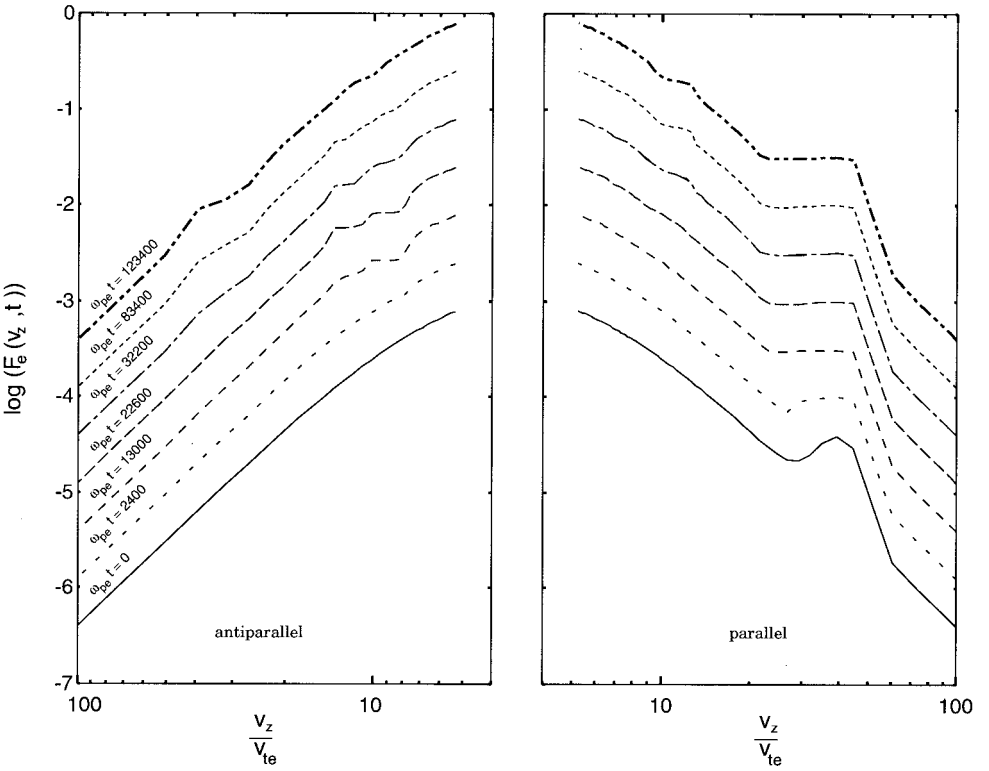

Figure 5. Time evolution of the reduced electron velocity distribution. The curves are shifted from each other for clarity.

space using the resonance condition $v_z \approx \omega_{pe}/k_z$ assuming $k_z\lambda_e \ll 1$, which is consistent with our wave spectra). The front edge of the surface is the initial condition for the k-space reduced electron distribution, identical to that in Figure 2b. Points closer to the center of the k_z axis correspond the high-velocity tails, while points at the outer edges correspond to the bulk of the electron distribution. On the front edge the notch to the right is the initial electron beam. The color of the surface represents the log of the wave power at a particular k_z and t, integrated over $k_\perp$. Plate 2 shows this same surface from the "bird's-eye" and "edge-on" perspectives. As time evolves (i.e., moving along the depth axis of the surface from front to back), the beam-resonant waves grow (magenta) while the beam flattens. The beam-resonant modes then backscatter to the left side of the surface (localized green regions). The waves at beam resonance become less intense (blue), while the backscattered waves flatten the electron distribution in the direction antiparallel to the beam (the plateaus on the left-hand part of the back edge of the surface). These antiparallel plateaus correspond to the two small notches in the reduced electron distribution plot in velocity space (Figure 5). Notice also the green region just to the right of the two plateaus. This is the on-axis backscatter. The fact that the on-axis backscatter occurs a few hundred plasma periods (ω_{pe}^{-1}) later than the off-axis backscatter may be due to the fact that the off-axis modes are at lower parallel phase velocities and therefore deform the electron distribution more readily (since $D \propto 1/v_z$), causing the damping rate to decrease, allowing for higher levels of wave energy [*Sanbonmatsu et al.*, 2000a].

The full 2-D Langmuir spectra are shown in Figure 6, which displays the spectra near-the-initial (Figure 6a), transient (Figure 6b), transition to steady state (Figure 6c), and steady state (Figure 6d) stages. The Langmuir wave spectra are interpreted in terms of wave-wave backscatter, which refers to a common channel of nonlinear wave-wave scattering as described by (9)–(10) [*Goldman*, 1984]. The backscatter instability occurs when a forward propagating beam-resonant Langmuir wave with frequency ω_0 and wave number k_0 scatters off ion acoustic density fluctuations with frequency ω_{ia} and wave number $k_{ia} = 2k_0 - k^*$ ($k^* \equiv \frac{2}{3}\sqrt{m_e/m_i}\lambda_e^{-1} \ll k_0$ due to wave-vector matching), producing a downshifted backward propagating daughter Langmuir wave with frequency $\omega_0 - \omega_{ia}$ and wave number $-k_0 + k^*$. The backscatter instability is a Stokes process (i.e., the daughter Langmuir wave is downshifted in frequency relative to the beam-driven wave). Coupled to the Stokes decay is a weaker forward scattering anti-Stokes interaction, where the original incident forward propagating Langmuir wave couples to the ion acoustic response at $2k_0 - k^*$, producing an upshifted forward scattered Langmuir wave with frequency $\omega_0 + \omega_{ia}$ and wave number $k_0 + k_{ia} = 3k_0 - k^*$. Although the anti-Stokes wave is nonresonant and heavily Landau damped, and therefore of low amplitude, it nevertheless can cause significant electron quasi-linear diffusion since the forward scattered waves are at high k and resonate with electrons at low velocity (recall that the diffusion coefficient is proportional to $1/v$).

3.3. Stage 1: Initial Transient

Figure 6a displays the early 2-D k-space wave spectrum of the Langmuir wave envelope in the linear stage of the bump-on-tail instability ($\omega_{pe}t = 2400$). Since the oblique modes are close to parallel, the perpendicular axis has been expanded by a factor of 6. Wave power has developed near the beam wave number $k_z \approx k_b$ and has a finite extent in k_z due to the finite

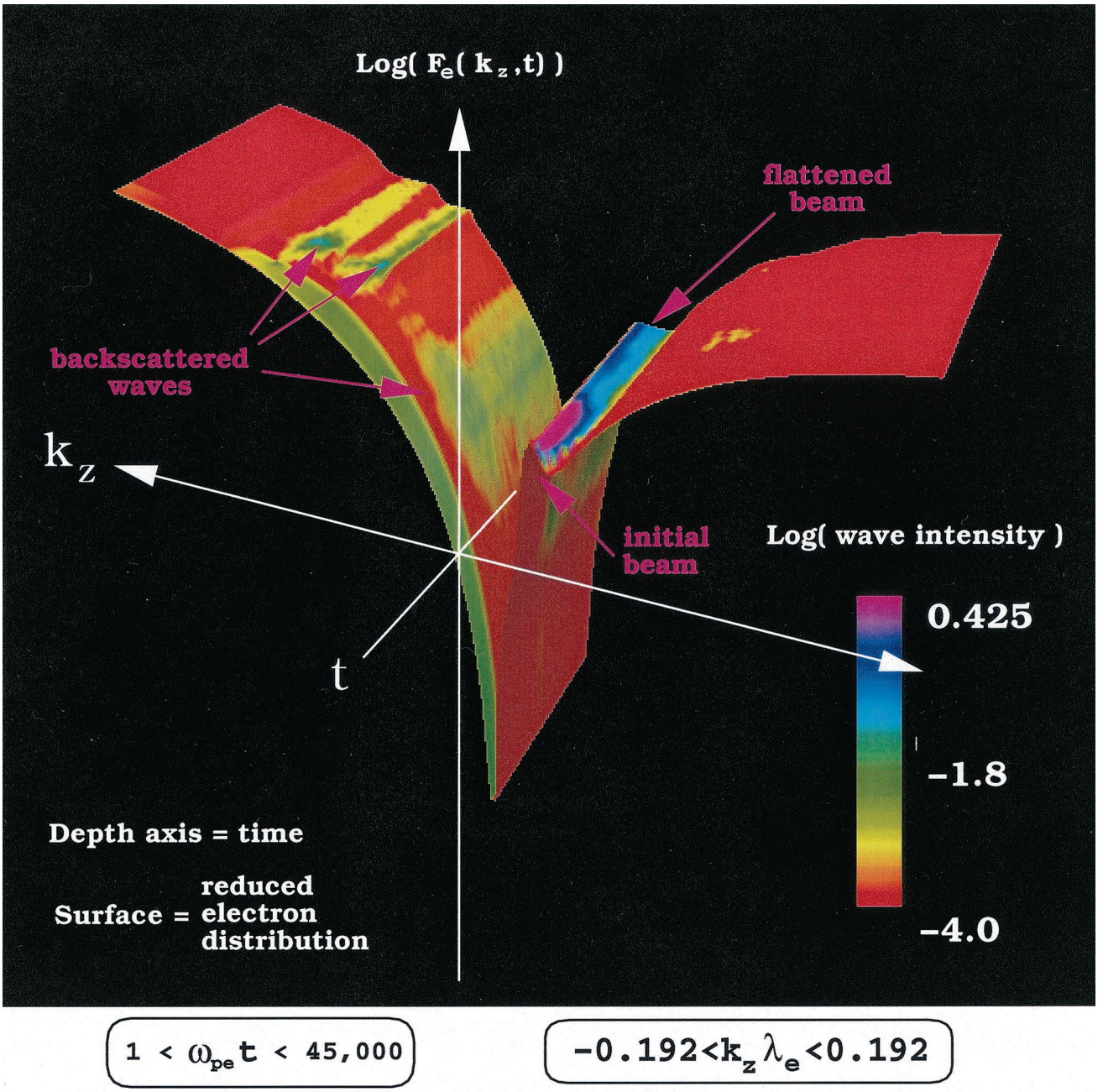

Plate 1. Time history of both the reduced wave spectrum and reduced electron distribution. The horizontal axis is parallel wave number k_z. The depth axis is time. The log of the wave power (integrated over $k_\perp$) is represented by color and plotted on the (k_z, t) plane. The log of the reduced electron distribution is represented by the surface level and plotted over the (k_z, t) plane. The green band at the front edge of the surface is the initial noise.

width of the beam. Doppler damping by the halo component of the electron distribution limits the perpendicular extent of the wave spectrum. The widths of the spectra are easily understood upon examination of Figures 3a and 3b. The beam-resonant waves react back on the electrons, flattening the reduced electron distribution via quasi-linear diffusion (Figure 5, $\omega_{pe}t$ = 2400).

The small amount of wave power on the left-hand side of Figure 6a satisfies the kinematic matching conditions for backscatter of beam-excited Langmuir waves off ion acoustic waves to backscattered Langmuir waves with phase velocities antiparallel to the beam. These antiparallel modes indeed grow at later times, as shown in Figure 6b, which displays the Langmuir wave spectrum at time $\omega_{pe}t$ = 13,000. The sideways "V" shape corresponds to contours of the magnetized Langmuir wave dispersion relation. We note that at lower altitudes where $\omega_{ce} < \omega_{pe}$ ("subcritical") the topology of the Langmuir dispersion surface $\omega(k_z, k_\perp)$ changes. In this case a single lobe (in the antiparallel direction) extended in k_z and centered around $k_\perp = 0$ would be expected rather than the two lobes which occur in our simulations for $\omega_{ce} > \omega_{pe}$ ("supercritical") [*Newman et al.*, 1994b].

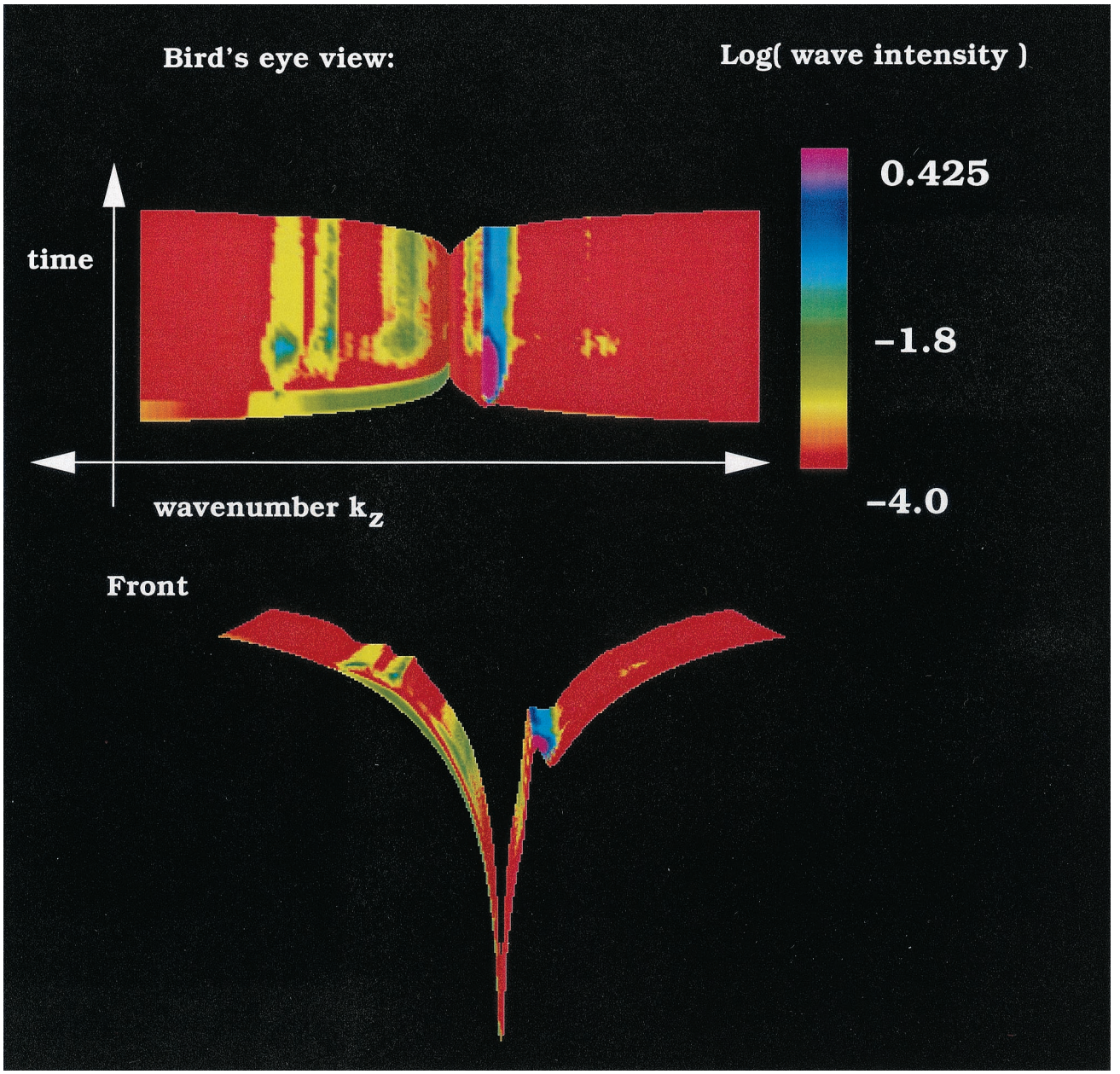

Plate 2. Same surface as in Plate 1 viewed from the bird's-eye and edge-on perspectives.

The wave power near $k_z = -k_b$ on axis ($k_\perp \approx 0$) is analogous to the well-studied 1-D backscatter. The far-off-axis-scattered modes (i.e., those in the lobes of the "V" with $k_\perp \neq 0$) have frequencies close to the on-axis backscattered modes. By this time ($\omega_{pe}t = 13{,}000$) the waves have exceeded the threshold for the backscatter instability, causing a large amount of backscatter. Seeing that the beam has flattened by this time (Figure 5), we conclude that wave-wave scattering and beam flattening occur simultaneously during $2400 < \omega_{pe}t < 13{,}000$. This is also demonstrated in Plate 2. The two small notches in the electron distribution near $v_z \approx -10v_e$ and $v_z \approx -15v_e$ are caused by quasi-linear diffusion due to the backscattered waves. Since the quasi-linear diffusion is proportional to v^{-1}, particles with lower velocities are more susceptible to diffusion. Thus even very low levels of backscattered waves are capable of diffusing the electron distribution at these lower velocities. These notches are more prominent by $\omega_{pe}t = 22{,}600$ (Figure 5) and can be seen clearly in k space in Plate 2.

Note that these notches at lower velocities (higher parallel wave number) do not occur in 1 D for $\omega_{ce} > \omega_{pe}$. Recall that scattering to higher wave numbers in 1 D is not kinematically permitted and violates energy conservation since the Langmuir frequency increases with wave number. In 2-D for $\omega_{ce} > \omega_{pe}$, however, the magnetic correction causes the Langmuir frequency to decrease with angle to the magnetic field $\bar{\theta}$. As long as the waves are scattered to sufficiently large $k_\perp$, scattering to higher k_z is permitted.

The wave-particle interaction timescale is estimated by the change in kinetic energy with time $t_{wp}^{-1} \approx 10000\omega_{pe}^{-1}$. This is distinguished from the quasi-linear diffusion time $t_D^{-1} \approx \partial_t F_e(v_z, t)/F_e(v_z, t)$, which is the time it takes for particles to diffuse out of the wave spectrum (discussed below). The timescale for wave-wave interactions is estimated from the time

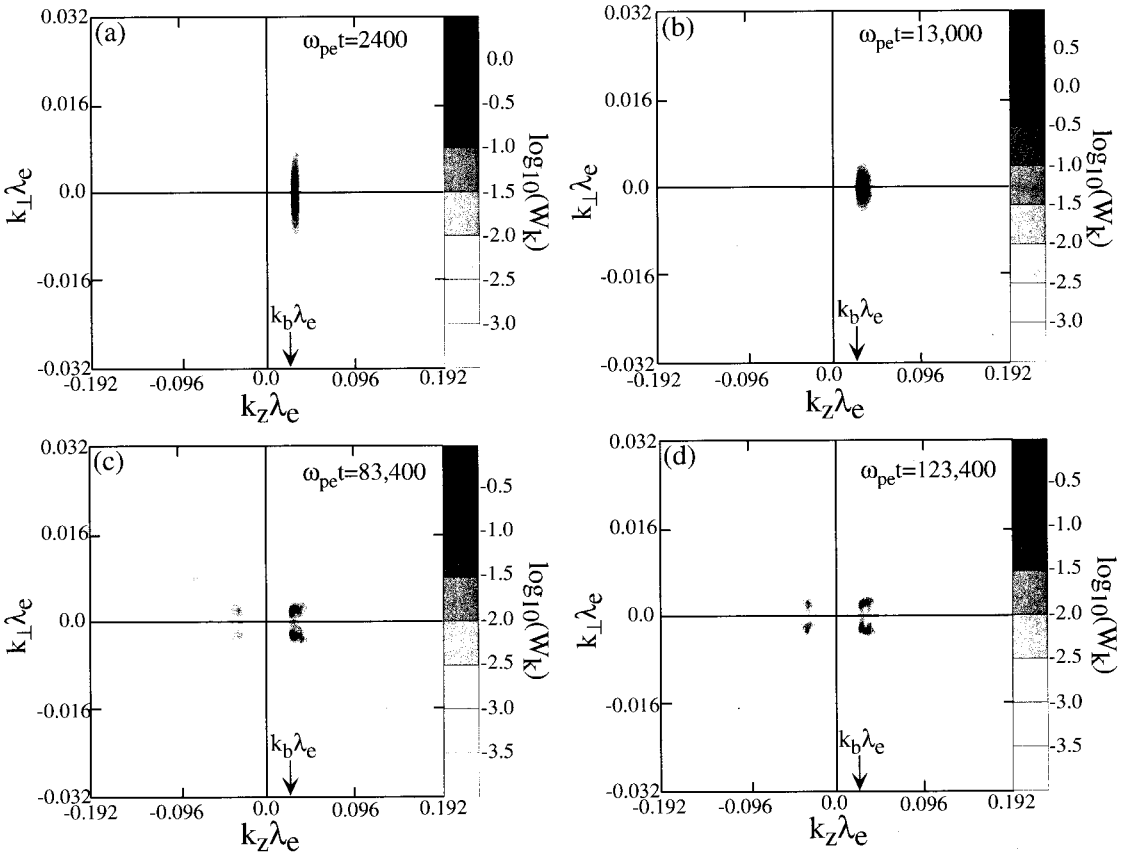

Figure 6. Two-dimensional wave spectrum for the Langmuir wave envelope potential for the (a) near-initial, (b) transient, (c) transition to steady state, and (d) steady state stages.

rate of change of average Langmuir wave energy. As the wave energy increases because of excitation by the positive velocity slope of the beam, the particle energy decreases because of beam flattening by the waves. Scattering occurs between $t = 2400\omega_{pe}^{-1}$ and $t = 13{,}000\omega_{pe}^{-1}$, before the beam has completely flattened, as evidenced by Figures 5 and 6b and Plate 2. Since the Langmuir wave growth rate is close to the bump-on-tail instability growth rate, we conclude that during this time the growth rate due to the beam sets the dominant timescale and is much greater than the depletion rate due to wave-wave scattering. Subsequently, wave energy levels exceed the threshold for wave-wave scattering, which takes wave energy away from beam-resonant phase velocities to low velocities, where it is transferred to the bulk of the electron distribution via wave-particle interactions (i.e., quasi-linear diffusion). The net effect is the depletion of Langmuir wave energy. This depletion occurs with decay rate $(\Delta W/\Delta t)/W$, where W is the dimensionless wave energy density $W = |E|^2/8\pi n_0 T_e$. The wave-wave timescale is determined from the inverse of the decay rate for times $11{,}000 < \omega_{pe}t < 13{,}000$, after the beam-resonant mode growth rate has decreased significantly. The timescale for wave-wave interactions is estimated to be $t_{ww} \approx 5000\omega_{pe}^{-1}$, comparable to the wave-particle timescale.

We emphasize that both of these timescales actually change with time throughout the simulation. At early times the wave-particle interactions occur much faster than the wave-wave interactions since the beam still has a steep slope and since the wave power is relatively low (the scattering rate is proportional to the wave power). At later times the wave-particle interactions slow because of beam flattening, while the wave-wave interactions speed up as a result of the large wave levels present. Thus, to obtain a realistic evolution of either the electron distribution or the wave spectrum, neither wave-particle interactions nor wave-wave interactions may be neglected.

The importance of including both wave-particle and wave-wave effects is shown in Figure 7. Here we compare two simulations for similar parameters to those used above. The first ("self-consistent") is similar to the above simulations in that it includes the self-consistent coupling of the quasi-linear diffusion equation and the Zakharov equations. This simulation, however, neglects the beam replenishment term. The second simulation ("fixed particle distribution") fixes the electron distribution and only evolves the wave spectrum, neglecting any quasi-linear wave-particle effects. Since the growth rate of the later simulation is fixed and does not decrease with time, the waves grow to a much higher level, inconsistent with spacecraft observations (discussed in section 3.5). Furthermore, the wave-wave timescale is much faster ($t_{ww} = 1500\omega_{pe}^{-1}$) for the simulation that is not self-consistent.

We note that the quasi-linear diffusion approximation is indeed valid. To demonstrate this, we consider the time for which the waves are at maximum $\omega_{pe}t \approx 10{,}000$ since this is the most likely time for the approximation to break down. At this time the parallel spectral width is $\Delta k_z\lambda_e \approx 0.0045$, giving a phase velocity width of $\Delta v_{\phi,z} \approx 5.5v_e$, using $k_z\lambda_e \approx 0.0285$ (the wave number at which the wave power is maximum). The diffusion coefficient is $D_{zz} \approx 0.49v_e^2\omega_{pe}$ (obtained numeri-

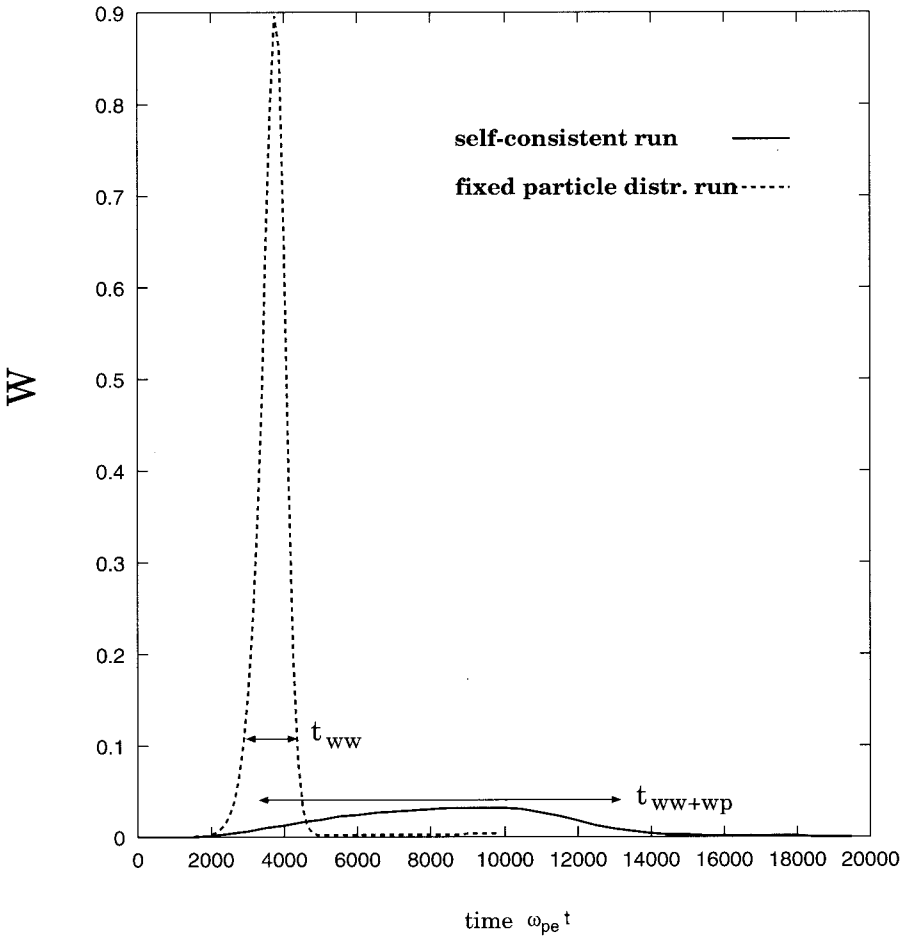

Figure 7. Comparison of self-consistent simulation with a simulation which fixes the electron distribution and only evolves the waves. The dashed curve represents the wave energy for the simulation that is not self-consistent. The solid curve is the self-consistent simulation.

cally from the simulation). This gives a quasi-linear diffusion time of $t_D = (\Delta v_{\phi,z})^2/2D_{zz} \approx 31\omega_{pe}^{-1}$. The autocorrelation time for this spectrum is $t_{ac} = 1/k_z\Delta v_{\phi,z} \approx 6.3\omega_{pe}^{-1}$, where we have again used $k_z\lambda_e \approx 0.0285$. Thus $t_D/t_{ac} \approx 5$, and the quasi-linear approximation is valid. This approximation is satisfied for the backscattered modes as well.

Returning to the wave history (Figure 4), we see that the instability has saturated by $\omega_{pe}t = 20{,}000$. Without beam replenishment the waves would decay to zero shortly after $\omega_{pe}t = 20{,}000$ (Figure 7). However, the beam replenishment term attempts to restore the beam to its original form, allowing it to maintain a small, but finite, positive slope, in turn maintaining the wave levels.

3.4. Stage 2: Near-Steady State

Because the plateaus in the backward direction are not completely flat, there is still a finite damping rate at wave numbers corresponding to these velocities. Thus the waves which created these plateau features eventually diminish, as seen at the final time presented in Plate 1, where the green scattered waves have changed to yellow. We can also see this in the k-space wave spectrum at time $\omega_{pe}t = 83{,}400$ (Figure 6c). Turning to the particles, we see in Figure 5 that the backward plateaus have become less prominent. This is due to the replenishment effect. Note that since the replenishment term is proportional to v_z, it takes longer to restore the electron distribution at these low velocities than it does to restore the beam. Also notice the small increase in the reduced electron distribution near $v_z \approx -40v_e = -v_b$. This is due to scattered waves with parallel wave numbers $k_z \approx -k_b$. As mentioned in section 3.2, diffusion is proportional to v_z^{-1}, so that diffusion at lower wave numbers and higher velocities occurs more slowly. So we only now begin to see the effect of the waves with $k_z \approx -k_b$ on the reduced electron distribution. Furthermore, there is a small amount of wave power near $k_z \approx 3k_b$. This is an order of magnitude below even the low-level backscattered modes. However, since it occurs at such high k_z, it does influence the reduced electron distribution at late times. This feature is due to the interaction between the primary beam-excited modes at $k_z \approx k_b$ and the density perturbations which are excited during the initial backscatter. Recall that for backscatter the daughter Langmuir wave has $k_{\text{scat}} \approx -k_b$. Kinematic wave vector matching (i.e., conservation of momentum) requires the ion acoustic density perturbation to have a wave number such that $k_{ia} \approx 2k_b$. This can interact with the initial beam mode to produce Langmuir waves at $k_z \approx k_b + k_{ia} \approx 3k_b$. The off-axis anti-Stokes modes are due to the interaction between the density perturbations near $k_{ia} \approx 2k_b$ and off-axis beam-excited modes.

We can see from the wave history (Figure 4) that the spatially averaged wave energy has essentially reached a steady

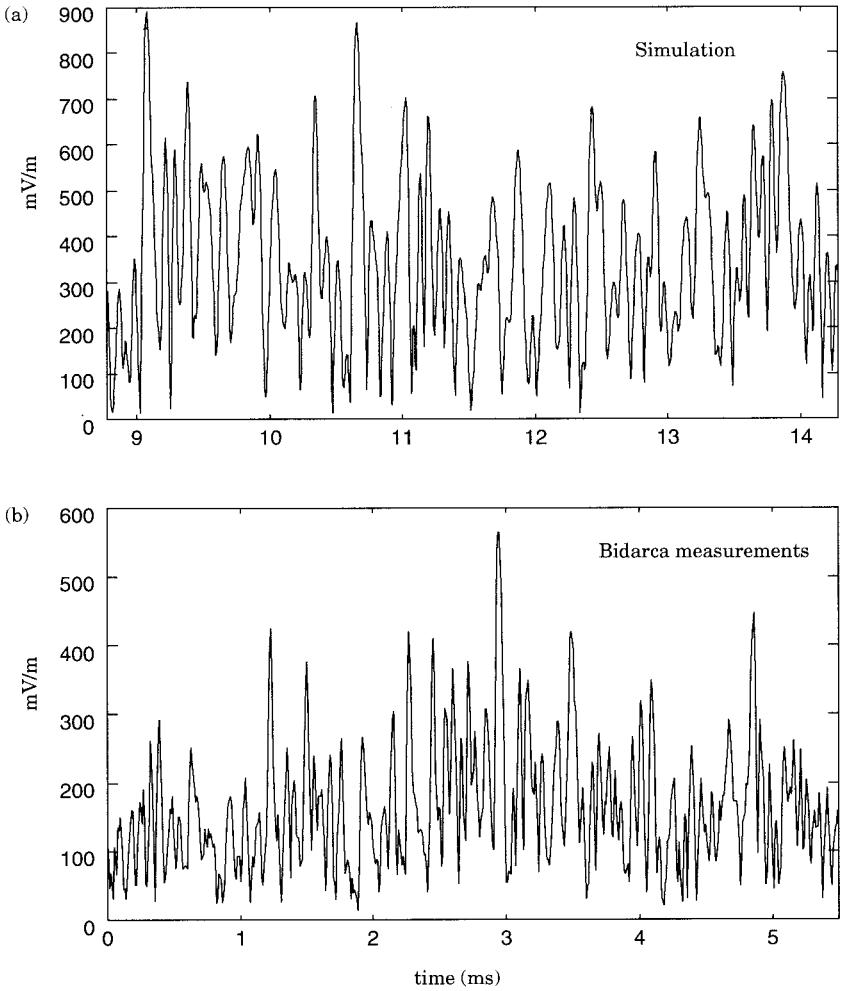

Figure 8. (a) Time history of the electric field envelope at a fixed spatial point in the simulation in physical units. (b) Time history of the electric field envelope as measured by the Bidarca spacecraft for a similar time interval to that in Figure 8a.

state by $\omega_{pe}t > 50{,}000$. By $\omega_{pe}t = 123{,}400$ the wave spectrum and reduced electron distribution have reached a near steady state. The wave spectrum steady state consists of the beam-excited modes ($k_z \approx k_b$), the backscattered modes ($k_z \approx -k_b$), and the low-level anti-Stokes modes near $k_z \approx 3k_b$ discussed above (Figure 6d). Our final 2-D k-space spectrum is similar to that determined by *Newman et al*. [1994b]. The reduced electron distribution has also reached a near-steady state (Figure 5), which consists of the flattened beam, the shoulder at $v_z \approx -v_b$ due to backscatter, and the small shoulder (which is now more prominent) near $v_z \approx v_b/3$ due to forward scattered anti-Stokes Langmuir waves.

On the whole, the near-steady state is a balance between wave-wave effects, wave-particle effects, and beam replenishment. The beam replenishment excites beam-resonant waves which are dissipated via quasi-linear diffusion at phase velocities near $v_z \approx v_b$ and via wave-wave backscatter to phase velocities that are not beam resonant. Ultimately, the backscattered waves are absorbed by the electrons at $v_z \approx -v_b$. All three effects are critical in obtaining the steady state. With no beam replenishment the waves would damp away (Figure 7). With no backscatter the waves would grow to very high levels. With no quasi-linear diffusion the waves would grow to very high levels, scatter, and be damped away by the electron halo component (Figure 7).

3.5. Comparison With Observations

While the Langmuir waves and electron distributions vary over a wide range in the auroral ionosphere, we use, as our guide, observations made on board the Bidarca sounding rocket which were presented by *Boehm* [1987], *Ergun et al*. [1993], and *Newman et al*. [1994b]. One particular Langmuir wave event was discussed by both *Boehm* [1987] and *Newman et al*. [1994b], which presented a 7 ms segment of the Langmuir wave envelope time history. This is shown in Figure 8 together with our simulation results. The typical burst duration was approximately 20–40 ms [*Ergun et al*. 1993].

Before comparing our wave simulation results with observations, we remind the reader that we are simulating plasma turbulence, which is random by its very nature. Thus we do not attempt to generate an exact fit to the observed wave histories and frequency spectra. Rather, we attempt to generate Langmuir turbulence whose general characteristics are consistent with the set of many spacecraft observations made near these altitudes. These characteristics are the typical amplitude of the

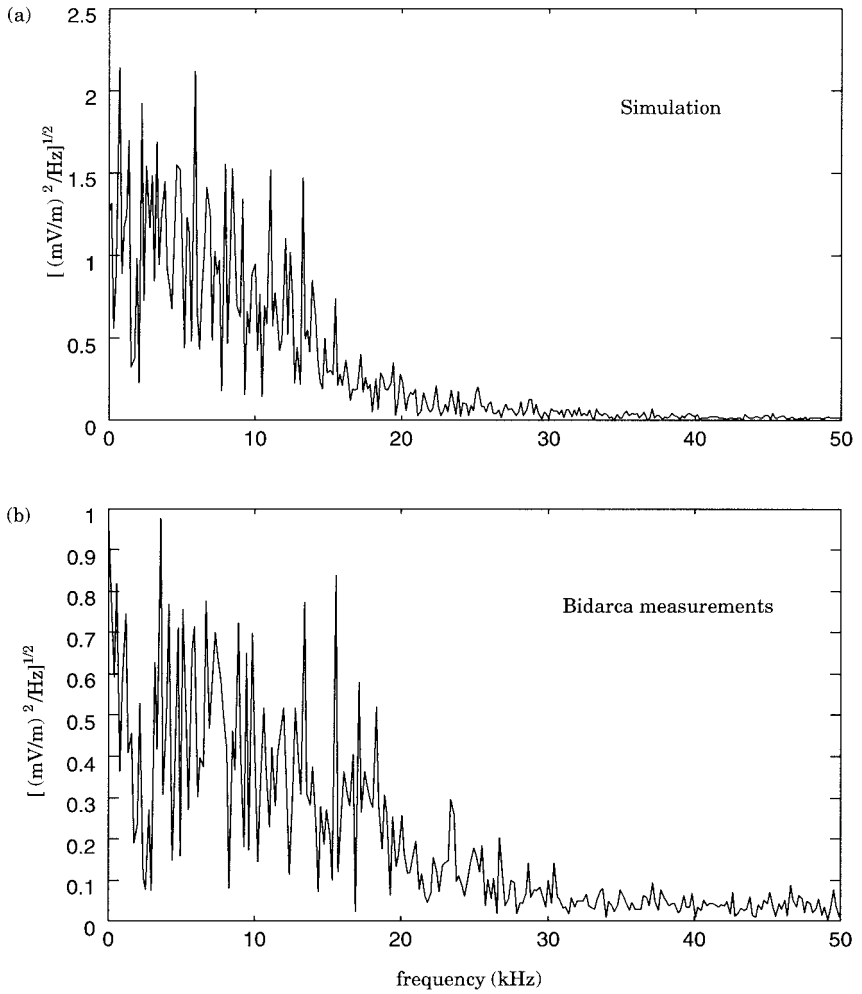

Figure 9. Envelope frequency spectra. (a) Temporal Fourier transform of the simulation electric field envelope for the time interval presented in Figure 8a. (b) Temporal Fourier transform of the measured electric field envelope for the time interval presented in Figure 8b.

Langmuir wave envelope and the typical modulation frequency.

Figure 8a presents a 5.5 ms sample of the time history for the electric field envelope at a fixed spatial point in our simulation in physical units. Figure 8b shows a 5.5 ms sample of the time history for the electric field envelope observed by Bidarca. We see that the typical wave amplitude in the simulation is approximately 500 mV m^{-1}. The typical measured amplitude for the Bidarca sample is approximately 250 mV m^{-1}. Observers have reported amplitudes as high as 1 V m^{-1} [*Stasiewicz et al*., 1996], though at higher altitudes. The differences between the simulation results and observations are discussed in detail in section 4.

Figure 9 displays the temporal Fourier transforms of the signals shown in Figure 8. Figure 9a is the simulation result, and Figure 9b is the measured result. These transforms of the Langmuir wave envelope are the modulation frequency spectra. The width of the modulation frequency spectrum is related to the width of the k-space spectrum in Figure 6d after being mapped from **k** to ω by the Langmuir wave dispersion relation. Physically, waves with different **k** have different frequencies and beat to produce modulations. The broader the spectrum in k space is, the more possible combinations of different frequencies there are, and hence the broader the modulation frequency spectrum is. From Figure 9 we see that the simulation modulation frequency spectrum is slightly narrower than the observed modulation frequency spectrum but is nevertheless in reasonable agreement.

Figure 10 shows the final simulation reduced electron energy distribution for comparison to a Bidarca reduced electron distribution presented in Figure 5c of *Ergun et al*. [1993] (shown in Figure 11 of this paper). Note that the observed shoulder features have negative slope, as opposed to the slight positive slope in our simulations. Because of the limited time resolution in the particle detectors (256 ms energy sweep period) the long integration time would be expected to average out the positive slope associated with transient features of the distribution as well as substantially weaken the shoulder feature. Reduced electron distributions with large positive slopes, such as that used as the initial condition in our simulation (Figure 2), would probably be unobservable because these features only last for $\sim 10{,}000\omega_{pe}^{-1}$ or 1.7 ms. In the simulation the large forward, or parallel, plateau is the flattened beam with energy E_b corresponding to v_b. The backward, or antiparallel, plateau near E_b in the backward direction (corresponding to $-v_b$) is due to the backscattered Langmuir waves. The secondary parallel plateau

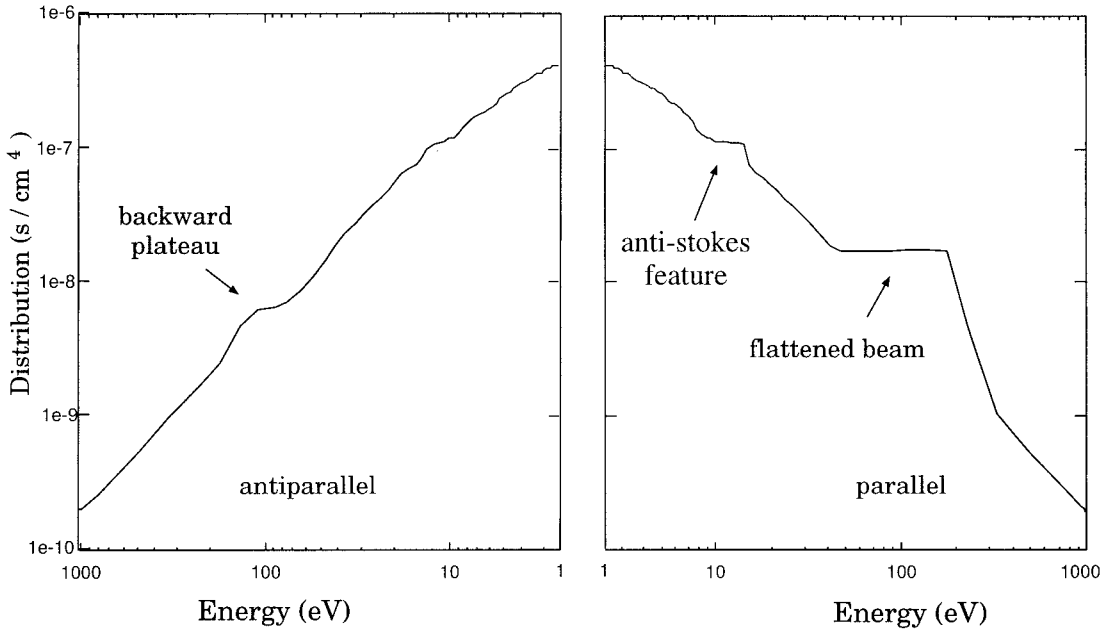

Figure 10. Reduced electron energy distribution at late times during the simulation. Read 1e-6 as 1×10^{-6}.

is due to the weak forward scattering. This plateau is near an energy of $E_b/9$, corresponding to a velocity of $v_b/3$ because of the forward scattering process described in section 3.2. Thus the ratio of the primary parallel to antiparallel plateau energies is approximately 1. The ratio of the secondary parallel to primary plateau energies is approximately 1/9. We expect to see plateaus at these ratios in observed reduced electron distributions. The energy ratio of the two forward plateau energies is consistent with the observed reduced electron distribution. However, no antiparallel reduced electron distribution was presented by *Ergun et al*. [1993]. We emphasize the need for a statistical study of shoulder features in reduced electron distributions in the parallel and antiparallel directions.

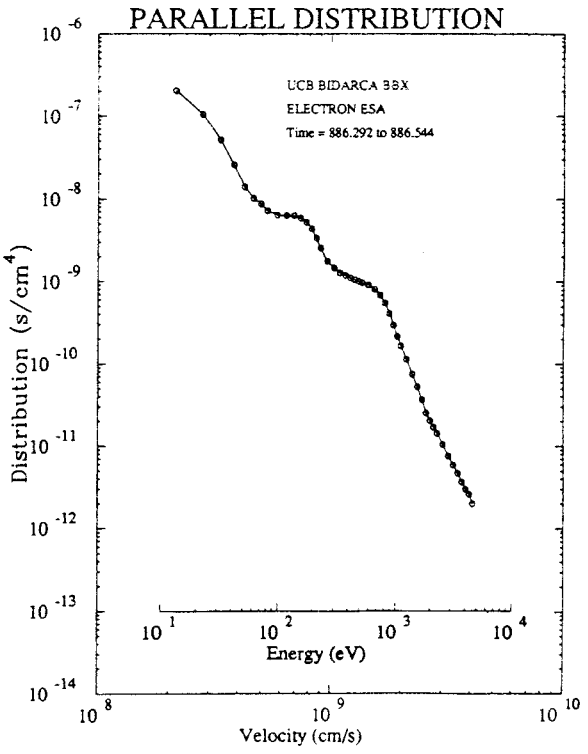

Figure 11. Reduced 1-D electron distribution measured by the Bidarca sounding rocket from *Ergun et al*., 1993, Figure 5c. Courtesy R. E. Ergun.

4. Discussion

We have constructed a quasi-linear Zakharov model which evolves the spatially averaged reduced electron distribution and magnetized Langmuir wave spectrum self-consistently. Simulations based on this model include wave-wave and wave-particle nonlinearities as well as advective beam replenishment.

The balance between the counteracting influences of quasi-linear diffusion, which tends to destroy the unstable positive slope in the precipitating "beam" electron distribution, and advective replenishment, which tends to restore the instability, can result in steady state turbulence with wave levels comparable to those observed by sounding rockets. The weak beam replenishment maintains a marginally unstable plateau-like distribution, which results in a very small Langmuir wave growth rate. This slow deposition of energy is balanced by the loss of wave energy via wave-wave scattering into Landau damped modes and quasi-linear diffusion of the electron distribution. It is specifically these weak steady wave growth rates that necessitate an efficient two-timescale kinetically self-consistent simulation method, such as the one employed in this study. Fully kinetic simulations (e.g., PIC codes) need stronger drivers in order to overcome noise and run time constraints. However, stronger drivers inevitably result in unphysically large wave intensities.

While our runs were very long from the perspective of 2-D kinetic plasma simulations ($>10^5\omega_{pe}^{-1}$), the physical times represented (approximately tens of milliseconds) are comparable in length to some observed Langmuir wave bursts. One consequence of these long weakly driven runs is the formation

of secondary plateaus in the evolved distribution function. In particular, these simulations produced a backward plateau with an energy near that of the primary forward plateau, as well as a secondary forward plateau with an energy of approximately 1/9 of the primary plateau. This finding suggests a possible generation mechanism for multiple plateaus observed in measured electron distributions.

In our simulations the antiparallel plateau is due to the backscatter of beam-excited Langmuir waves off an ion acoustic density response. Because the wave-wave and wave-particle interaction timescales are on the same order, the backscattered Langmuir waves are able to flatten the electron distribution in the backward direction via quasi-linear diffusion, creating the backward, or antiparallel plateau. The secondary forward parallel plateau is the result of the beam-excited Langmuir waves coupling to the ion acoustic density fluctuations created by the original backscatter. The ion acoustic waves produced in our simulations at $k_{ia} \approx 2k_b$ have frequencies of approximately 300 Hz. ELF wave power near this frequency has been observed by Alaska 93 [*Delory*, 1996].

The simulation parameters were varied extensively, and the qualitative results presented in section 3 prove to be robust, occurring in a wide range of parameter sets. For example, in another simulation run the initial beam and halo density were approximately doubled ($n_b/n_0 = 0.0011$ and $n_H = 0.065n_0$), the beam velocity was decreased ($v_b = 35v_e$), and the replenishment length was halved ($L = 360{,}000\lambda_e$). This run had a very similar initial transient stage, with beam-excited Langmuir waves backscattering to on-axis and off-axis modes, resembling Figure 6b. The wave spectrum relaxed to a similar state to that in Figure 6d. The reduced electron distribution showed similar features in the backward and forward directions during both the initial and near–steady state stages of the simulation. The timescales were also similar. In fact, simulation runs for a wide range of halo densities, beam densities, beam velocities, and replenishment lengths gave essentially the same qualitative results. The results were independent, both qualitatively and quantitatively, of grid cell size and time step, provided both were sufficiently small. Increasing the initial noise level caused the instability to begin sooner.

Quantitatively, the steady state wave levels depend on a combination of the beam density n_b, beam replenishment length L, and halo density n_H. Variation of the beam replenishment length L causes the wave levels to increase or decrease. Shorter replenishment lengths result in stronger beam replenishment and higher wave levels for a given beam density. For a given replenishment length, higher beam densities will result in higher steady state wave levels. However, a simulation with a relatively high beam density but very long replenishment length can result in lower wave levels than one with a very tenuous beam but with a short replenishment length. While many combinations of n_b and L result in the same steady state wave levels, the wave levels are more sensitive to beam density than replenishment length. Upon performing simulations for various values of n_b and L, we found that while L must be increased by a factor of $\approx$5 to decrease the wave levels by a factor of 2, the beam density n_b only needs to be decreased by a factor of $\approx$1.5 to decrease the wave levels by a factor of 2.

The modulation frequency is also affected by the replenishment length and beam density. This can be understood by studying Figure 3b (the initial growth rate versus $k_\perp$). When this curve is plotted for many different values of beam density, it is easy to see that the perpendicular width of the growth rate depends on the maximum growth rate. Lower beam densities give narrower regions of growth in $k_\perp$ and hence narrower modulation frequency spectra. Likewise, higher beam densities result in wider modulation frequency spectra. Decreasing the replenishment length effectively increases the growth rate, as described above. This, in turn, results in a wider modulation frequency spectrum. However, as with the wave amplitudes, the modulation frequency is less sensitive to replenishment length than to beam density.

The effect of changing the halo density is more complicated. Decreasing the halo density n_H has two effects. The most obvious effect is to decrease Cerenkov damping and allow higher levels of beam-resonant Langmuir waves. The second effect is more subtle. Decreasing the halo density also has the effect of widening the k-space Langmuir spectrum in the perpendicular direction, since the halo component of the reduced electron distribution also controls the Doppler damping. Since the Langmuir frequency is much more sensitive to $k_\perp$ than to k_z, it is the perpendicular width of the k-space spectrum that controls the width of the frequency spectrum. Increasing the perpendicular width of the k-space spectrum increases the range of frequencies of the Langmuir waves in the simulation. The beating of waves of many different frequencies results in a relatively fast typical modulation frequency of the Langmuir wave envelope. Thus decreasing the halo density results in faster typical modulation frequencies. Since a more tenuous halo also allows for higher wave levels, it is difficult to obtain a desired amplitude and typical modulation frequency simultaneously.

The main reason why our simulation wave amplitudes exceed the observed amplitudes is the complicated dependence of the wave amplitudes and modulation frequency spectra on the halo density n_H, beam density n_b, and replenishment length L. Attempting to decrease the amplitudes further by increasing the replenishment length, decreasing the beam density, or increasing the halo density narrows the modulation frequency spectrum, resulting in much slower modulations than those in the Bidarca event in question. Other wave events have been observed, however, with these slower modulations [*Boehm*, 1987].

As mentioned in section 3.2, we ran our simulations out to a physical time of 47 ms, with a near-steady state occurring for times >4 ms, giving Langmuir wave power for 43 ms. This is consistent with the observed burst durations of 20–100 ms in the sense that the observed bursts also show Langmuir wave power for timescales of many tens of milliseconds [*Boehm*, 1987]. In its present form it is likely that our model results in a true steady state, which is inconsistent with Langmuir bursts of finite duration. To properly model such a finite length burst would require additional time dependencies in the source terms of our model (e.g., time-dependent beam parameters). For example, a beam velocity that decreases with time would model the typically observed velocity dispersion in field-aligned electrons more accurately [*Ergun et al.*, 1993]. This would cause the primary parallel shoulder to decrease in energy with time. As a result, the antiparallel shoulder and secondary parallel shoulder would also decrease in energy with time. The energy shift of the antiparallel and secondary parallel plateaus may be delayed with respect to the energy shift in the primary parallel plateau by the wave-particle interaction time ($\approx$2–4 ms). The inclusion of such time dependencies in the beam parameters would be an obvious extension for future simulation studies. The absence of this effect in our model may

be one possible cause of the larger wave amplitudes produced by our simulations in comparison to the observed wave amplitudes. If the beam density were gradually increased and subsequently decreased to mimic a burst, one would expect a lower total wave energy (integrated over the simulation time).

Another possible explanation of the difference between the simulation results and observations may be that our model does not include lower hybrid waves, which would provide an additional channel of decay for beam-excited Langmuir waves, resulting in lower Langmuir wave levels. We emphasize that our work is a first study of the competition between nonlinear wave-wave and wave-particle effects in the auroral ionosphere. As a first step, we have included as our wave-wave effects interactions between magnetized Langmuir waves and ion acoustic waves. A more complete study should include interactions between magnetized Langmuir waves, ion acoustic waves, and lower hybrid waves. It might be possible to construct a three-timescale Zakharov equation model accounting for coupling between Langmuir, ion acoustic, and lower hybrid waves; however, this would be difficult because of the broadband nature of lower hybrid waves. We also note that while there is strong evidence for lower hybrid waves at higher altitudes [*Stasiewicz et al*., 1996; *Bonnell et al*., 1997], the observational evidence for lower hybrid waves below 700 km is marginal.

Furthermore, side scatter off lower hybrid waves cannot produce Langmuir waves with significantly different phase velocities than the beam-excited Langmuir wave phase velocities. Thus one would not expect side-scattered Langmuir waves to produce distinct multiple shoulder features in the electron distribution consistent with observations. Shoulder features in the electron distribution antiparallel to the precipitating electron beam cannot be produced by coupling between Langmuir and lower hybrid waves because side scatter does not produce antiparallel Langmuir waves. We do not expect the inclusion of lower hybrid waves to effect our central conclusion, namely, that wave-wave interactions between Langmuir and ion acoustic waves are important in forming multiple shoulder features in the reduced electron distribution.

There are, of course, other possible explanations for multiple plateau features in observed reduced electron distributions. The most obvious contender would be the existence of multiple remote sources for accelerated precipitating field-aligned electrons. One may also consider spatial inhomogeneities to explain the multiple shoulders. That is, if the time interval over which the distribution is measured covers a period when the spacecraft moves from one domain to another, each having different beam characteristics, then one may observe multiple shoulders. However, this would not explain the antiparallel plateaus unless the beams happened to be propagating in opposite directions.

While our simulation parameters are reasonable, they are not universal. In principle, one should be able to find parameters which do not produce multiple shoulders. The fact that our simulations produce multiple shoulders which are somewhat consistent with observations suggests but does not prove that our model explains the observations. However, because our proposed mechanism makes specific predictions regarding the relative velocities of the various plateau features, it is possible, in principal, to test whether there is a clearly identifiable subset of distributions with multiple plateaus that are consistent with our model.

Acknowledgments. We wish to thank R. E. Ergun, G. T. Delory, and K. Lynch for valuable conversations regarding observed electron distributions. This research was supported by NSF grant ATM-9417116 and NASA grant ITM SR&T NAGW-4453. K. Y. Sanbonmatsu is currently supported by the United States Department of Energy.

Janet G. Luhmann thanks John W. Bonnell and another referee for their assistance in evaluating this paper.

References

Boehm, M. H., Waves and static electric fields in the auroral acceleration region, Ph.D. thesis, Dep. of Phys., Univ. of Calif., Berkeley, 1987.

Bonnell, J., P. Kintner, J. E. Wahlund, and J. A. Holtet, Modulated Langmuir waves: Observations from Freja and SCIFER, *J. Geophys. Res*., *102*, 17,233, 1997.

Clemmow, P. C., and J. P. Dougherty, Electrodynamics of particles and plasmas, Addison-Wesley-Longman, Reading, Mass., 1969.

Delory, G. T., Rocket observations of VLF bursts, electron precipitation, and ion heating in the auroral ionosphere, Ph.D. thesis, Dep. of Phys., Univ. of Calif., Berkeley, 1996.

Dum, C. T., and K. I. Nishikawa, Two-dimensional simulation studies of the electron beam-plasma instability, *Phys. Plasmas*, *1*, 1821, 1994.

Ergun, R. E., C. W. Carlson, J. P. McFadden, and J. H. Clemmons, Langmuir wave growth and electron bunching: Results from a wave-particle correlator, *J. Geophys. Res*., *96*, 225, 1991.

Ergun, R. E., G. T. Delory, E. Klementis, C. W. Carlson, J. P. McFadden, I. Roth, and M. Temerin, VLF wave growth from dispersive bursts of field-aligned electron fluxes, *J. Geophys. Res*., *98*, 3777, 1993.

Goldman, M. V., Strong turbulence of plasma waves, *Rev. Mod. Phys*., *56*, 709, 1984.

Kellogg, P. J., and S. J. Monsoon, Rocket observation of high frequency waves over a strong aurora, *J. Geophys. Res*., *83*, 47, 1978.

Kennel, C. F., and F. Engelmann, Velocity space diffusion from weak plasma turbulence in a magnetic field, *Phys. Fluids*, *9*, 2377, 1966.

Kintner, P. M., J. Bonnell, S. Powell, and Jan-Erik Wahlund, First results from the Freja HF Snapshot Receiver, *Geophys. Res. Lett*., *22*, 287, 1995.

Krasnoselskikh, V., and V. Sotnikov, Plasma wave collapse in a magnetic field, *Sov. J. Plasma Phys*., *Engl. Transl*., *3*, 491, 1977.

Lin, R. P., W. K. Levedahl, W. Lotko, D. A. Gurnett, and F. L. Scarf, Evidence for nonlinear wave-wave interactions in solar type-III radio-bursts, *Astrophys. J*., *308*, 954, 1986.

Mace, R. L., and M. A. Hellberg, A dispersion function for plasmas containing superthermal particles, *Phys. Plasmas*, *2*, 2098, 1995.

McFadden, J. P., C. W. Carlson, and M. H. Boehm, High frequency waves generated by auroral electrons, *J. Geophys. Res*., *91*, 12,079, 1986.

Muschietti, L., and C. T. Dum, Nonlinear-wave scattering and electron-beam relaxation, *Phys. Fluids B*, *3*, 1968, 1991.

Muschietti, L., I. Roth, and G. Delory, Oblique turbulence driven by field-aligned electron fluxes in the auroral ionosphere, *J. Geophys. Res*., *102*, 27,217, 1997.

Newman, D. L., R. M. Winglee, P. A. Robinson, J. Glanz, and M. V. Goldman, Simulations of the collapse and dissipation of Langmuir wave packets, *Phys. Fluids B*, *2*, 2600, 1990.

Newman, D. L., M. V. Goldman, R. E. Ergun, and M. H. Boehm, Langmuir turbulence in the auroral ionosphere, 1, Linear theory, *J. Geophys. Res*., *99*, 6367, 1994a.

Newman, D. L., M. V. Goldman, R. E. Ergun, and M. H. Boehm, Langmuir turbulence in the auroral ionosphere, 2, Nonlinear theory and simulations, *J. Geophys. Res*., *99*, 6377, 1994b.

Robinson, P. A., and D. L. Newman, Three-dimensional strong Langmuir turbulence and wave collapse, *Phys. Rev. Lett*., *61*, 702, 1988.

Robinson, P. A., and D. L. Newman, Two-component model of strong Langmuir turbulence: Scalings, spectra, and statistics of Langmuir waves, *Phys. Fluids B*, *2*, 2999, 1990.

Sanbonmatsu, K. Y., I. Doxas, M. V. Goldman, and D. L. Newman, Non-Markovian electron diffusion in the auroral ionosphere at high Langmuir-wave intensities, *Geophys. Res. Lett*., *24*, 807, 1997.

Sanbonmatsu, K. Y., H. X. Vu, D. F. DuBois, and B. Bezzerides, New paradigm for the self-consistent modeling of wave-particle and wave-wave interactions in the saturation of electromagnetically driven parametric instabilities, *Phys. Rev. Lett*., *82*, 932, 1999.

Sanbonmatsu, K. Y., H. X. Vu, B. Bezzerides, and D. F. DuBois, The effect of kinetic processes on Langmuir turbulence, *Phys. Plasmas*, *7*, 1723, 2000a.

Sanbonmatsu, K. Y., H. X. Vu, D. F. DuBois, and B. Bezzerides, Quantitative comparison of reduced-description particle-in-cell and quasilinear-Zakharov models for parametrically excited Langmuir turbulence, *Phys. Plasmas*, *7*, 2824, 2000b.

Shapiro, V. D., and V. I. Shevchenko, The nonlinear theory of interaction between charged particle beams and a plasma in a magnetic field, *Sov. Phys. JETP*, *Engl. Transl*., *15*, 1053, 1962.

Shapiro, V. D., and V. I. Shevchenko, Astrophysical plasma turbulence I, *Sov. Sci. Rev*., *Sect. E*, *6*, 425, 1988.

Stasiewicz, K., B. Holback, V. Krasnoselskikh, M. Boehm, R. Bostrom, and P. M. Kintner, Parametric instabilities of Langmuir waves observed by Freja, *J. Geophys. Res*., *101*, 21,515, 1996.

Thomson, J. J., R. J. Faehl, and W. L. Kruer, Mode-coupling saturation of the parametric instability and electron heating, *Phys. Rev. Lett*., *31*, 918, 1973.

Thomson, J. J., R. J. Faehl, W. L. Kruer, and S. Bodner, Electron heating due to parametric instability turbulence, *Phys. Fluids*, *17*, 973, 1974.

Zakharov, V. E., and A. B. Shabat, Exact theory of two-dimensional self-focusing and one-dimensional self-modulation of waves in nonlinear media, *Sov. Phys. JETP*, *Engl. Transl*., *34*, 62, 1972.

M. V. Goldman and D. L. Newman, Center for Integrated Plasma Studies, University of Colorado at Boulder, Campus Box 390, Boulder, CO 80309-0390. (goldman@spot.colorado.edu; david.newman@colorado.edu)

K. Y. Sanbonmatsu, Applied Theoretical and Computational Division, Los Alamos National Laboratory, MS B259, Los Alamos, NM 87545. (kys@lanl.gov)

(Received July 10, 2000; revised October 23, 2000; accepted October 27, 2000.)